

DOI: 10.1002/cbic.201300104

Theoretical Spectroscopy of the Ni^{II} Intermediate States in the Catalytic Cycle and the Activation of [NiFe] Hydrogenases

Tobias Krämer, Mario Kampa, Wolfgang Lubitz, Maurice van Gastel,* and Frank Neese*^[a]

[NiFe] hydrogenases catalyze the reversible oxidation of dihydrogen. The corresponding catalytic cycle involves a formidable number of redox states of the Ni-Fe active site; these can be distinguished experimentally by the IR stretching frequencies of their CN and CO ligands coordinated to iron. These spectroscopic fingerprints serve as sensitive probes for the intrinsic electronic structure of the metal core and, indirectly, for the structural composition of the active site. In this study, density functional theory (DFT) was used to calculate vibrational frequencies, by focusing on the EPR-silent intermediate states that contain divalent metal centers. By using the well-characterized Ni-C and Ni-B states as references, we identified candidates for the Ni-SI_r, Ni-SI_a, and Ni-R states by matching the predicted relative frequency shifts with experimental results. The

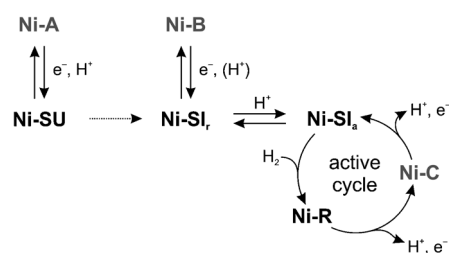
Ni-SI_r and Ni-SI_a states feature a water molecule loosely bound to nickel and a formally vacant bridge. Both states are connected to each other through protonation equilibria; that is, in the Ni-SI_a state one of the terminal thiolates is protonated, whereas in Ni-SI_r this thiolate is unprotonated. For the reduced Ni-R state two feasible models emerged: in one, H₂ coordinates side-on to nickel, and the second features a hydride bridge and a protonated thiolate. The Ni-SU state remains elusive as no unequivocal correspondence between the experimental data and calculated frequencies of the models was found, thus indicating that a larger structural rearrangement might occur upon reduction from Ni-A to Ni-SU and that the bridging ligand might dissociate.

Introduction

In a time when fossil fuels are becoming increasingly scarce, the need to switch to biorenewable energy sources becomes more and more apparent. Molecular hydrogen, H₂, is ideal for storing energy, given its relatively high energy density and its environmentally clean products of combustion. In nature, hydrogenase enzymes are able to produce H₂ from protons and electrons, with rates of up to 10 000 mol mol⁻¹ s⁻¹.^[1–4] The electrochemical properties and mechanisms of this class of enzyme have been investigated by many research groups, by both experimental^[5–11] and theoretical means.^[12–17]

Three classes of hydrogenase exist: [NiFe] hydrogenases, [FeFe] hydrogenases, and [Fe] hydrogenases.^[1] [NiFe] hydrogenase enzymes consist of two subunits. The large subunit contains the active [NiFe] center, which harbors nickel, iron, two bridging cysteines, two cysteines bound terminally to nickel, and three inorganic diatomic ligands (2CN⁻, 1CO) to iron.^[18–26] The small subunit contains three iron–sulfur clusters, which are believed to be part of the electron transport chain. The enzymes display surprisingly rich redox chemistry.^[27–31] Owing to the presence of the Fe-bound diatomic cyanide and carbon-

monoxide ligands, FTIR spectroscopy is exceptionally well-suited to monitor the redox states of the [NiFe] hydrogenases (and their changes), by monitoring these ligands' distinct stretching frequencies. About ten distinct states have been observed.^[32]



Scheme 1. The inactive states Ni-A, Ni-B, Ni-SU, and Ni-SI_r, and the active redox states Ni-SI_a, Ni-C, and Ni-R of the catalytic cycle of [NiFe] hydrogenase. Paramagnetic states are shown in red; EPR-silent states are in black. States become more reduced from top to bottom.

Scheme 1 shows a schematic overview of the redox states of the enzyme,^[33] as characterized by FTIR spectroscopy.^[29,30,34] Each state has a unique fingerprint (the stretching frequencies of the diatomic ligands), which depends somewhat on the particular enzyme.^[29,30] In the most-oxidized state, the enzyme is inactive.^[35] The experimentally observed frequencies for *Desulfovibrio vulgaris* Miyazaki F hydrogenase are shown in Table 1.^[34] Owing to the large crystal field splitting imposed by

[a] Dr. T. Krämer, Dr. M. Kampa, Prof. Dr. Dr. W. Lubitz, Dr. M. van Gastel, Prof. Dr. F. Neese

Max-Planck-Institut für Chemische Energiekonversion
Stiftstrasse 34-36, 45470 Mülheim an der Ruhr (Germany)
E-mail: maurice.van-gastel@cec.mpg.de
frank.neese@cec.mpg.de


 Supporting information for this article is available on the WWW under <http://dx.doi.org/10.1002/cbic.201300104>.

Table 1. Experimental FTIR frequencies [cm^{-1}] for the CO and CN vibrations in the [NiFe] hydrogenase of *D. vulgaris* Miyazaki F. Data reproduced from ref. [34]. The Ni-SI_r and Ni-R states are represented by the most abundant fingerprint at neutral pH. The values in brackets are the shifts with respect to Ni-C.

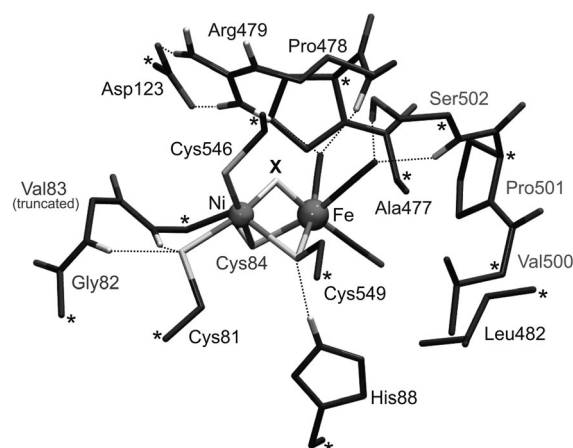
	Ni-A	Ni-B	Ni-C	Ni-SU	Ni-SI _r	Ni-SI _a	Ni-R
CO	1956 (−5)	1955 (−6)	1961	1958 (−3)	1921 (−40)	1943 (−18)	1948 (−5)
CN	2085 (+11)	2081 (+7)	2074	2089 (+15)	2061 (−13)	2074 (0)	2061 (−13)
CN	2094 (+9)	2090 (+5)	2085	2100 (+15)	2070 (−15)	2086 (+1)	2074 (−11)

the CN and CO ligands, the Fe ion resides in a formal divalent low-spin oxidation state and is not redox active in the catalytic cycle. The oxidized [NiFe] center is paramagnetic, and two distinct EPR spectra have been recorded. The states associated with these spectra are called Ni-A and Ni-B, both of which have been identified as Ni^{III} species.^[36–41] The enzyme can be activated by reducing the metal centers with H₂.^[7,27,42] For the Ni-A state, activation takes place on the timescale of minutes to hours, whereas the Ni-B state activates on the seconds timescale.^[43] For this reason, the Ni-A state is also called the “unready state” and Ni-B is called the “ready state”. During activation, the Ni-A and Ni-B states first become one-electron reduced. The ensuing EPR-silent states are still inactive, and are called Ni-SU (“silent unready”) and Ni-SI_r (“silent ready”); it is believed that the conversion from Ni-SU to Ni-SI_r is slow and constitutes the rate-limiting step for the activation of the unready state.^[31]

The Ni-SI_r state is believed to be in protonation equilibrium with Ni-SI_a (“silent active”),^[29,30] the most oxidized state that participates in the catalytic cycle. The other active states that form part of the active cycle are Ni-C (a paramagnetic state in which nickel is formally trivalent) and Ni-R (a diamagnetic state in which nickel is formally divalent).^[31] The relative abundances of the Ni-C and Ni-R states were found to be dependent on the partial pressure of H₂.^[27,31] Moreover, in some enzymes, up to three Ni-R states have been observed (Ni-R1, Ni-R2, and Ni-R3),^[31] the relative abundances of which depended on pH.

A unique feature of the [NiFe] hydrogenases is the bridging ligand (“X” in Figure 1). The identity of this bridging ligand depends on the redox state of the metal center. Its identity (in particular its nucleophilicity) influences the strength of the bond to iron, and consequently modulates the total electron density at the iron. This in turn affects the stretching frequencies of the diatomic ligands. In general, if electron density is increased at the iron, π backdonation into π^* anti-bonding orbitals of the diatomic ligands increases, thereby weakening the bonds of the diatomic ligands. The identity of the bridging ligand is in principle most easily determined by X-ray crystallography, provided it is possible to crystallize the protein in a pure redox state.^[18–26] Additional information (e.g., the protonation state of the ligand) can be obtained from spectroscopy, in particular EPR spectroscopy, for the paramagnetic intermediates,^[32,40–42,44–53] but also indirectly by the nucleophilicity of the ligand, to which the stretching frequencies of the diatomic ligands are sensitive.^[29,30,34]

For the EPR-active states Ni-B and Ni-C, a clear picture has arisen about the identity of ligand X. For Ni-B the crystal structure demonstrated the presence of an oxygen ligand, either

**Figure 1.** Cluster model of [NiFe] hydrogenase in the Ni-C state. α -C atoms that were fixed at their X-ray structure positions during geometry optimization are indicated by an asterisk. X represents the bridging hydride; hydrogen bonds are indicated by dotted lines. Amino acid residues are numbered as for the *D. vulgaris* Miyazaki F enzyme. Aliphatic hydrogen atoms are omitted for clarity.

O²⁻, OH⁻ or H₂O.^[25] EPR studies on single crystals and deuterium exchange experiments found that the ligand was singly protonated, thus identifying it as a hydroxo ligand.^[41] Moreover, the hydroxo ligand was found to be in one of two possible conformations, such that two lone-pair orbitals form bonds to the respective metals, and the third lone-pair points to a putative hydrogen channel.^[41] X-ray diffraction experiments using high pressure xenon gas suggested that molecular hydrogen travels through this channel from the protein surface to the metal center.^[19,54] For the Ni-C state, electron density at X was absent in the crystal data.^[23] However, Hyperfine Sublevel Correlation Spectroscopy (HYSCORE) in combination with deuterium exchange indicated the presence of a hydride ligand at X.^[48,51] For the other paramagnetic state, Ni-A, the identity of the ligand is still not resolved, although recent crystal structures again point to a ligand with only one oxygen atom.^[26]

FTIR spectroscopy is, in principle, also sensitive to the protonation state of the bridging ligand, as the stretching frequencies are expected to be quite different (depending on whether the bridging ligand is anionic or neutral). Moreover, the stretching frequencies of the diatomic ligands are accessible for all redox states. In combination with quantum chemistry, the experimentally observed stretching frequencies may be analyzed to investigate the identity of ligand X in all redox states.

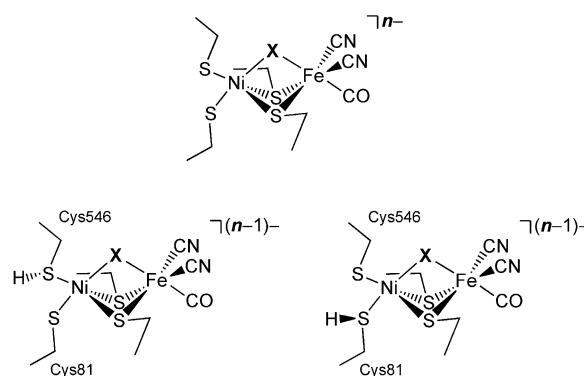
Many reports of quantum chemical calculations with emphasis on stretching frequencies of the diatomic ligands in [NiFe]

hydrogenases are present in literature, in particular from the Hall group.^[55,56] Early work focused on the Ni-A and Ni-SU states.^[56] This work made use of reference calculations that showed a correlation between the experimental CO stretching frequency and the calculated CO bond distance.^[55] This correlation was subsequently used for comparison of the calculated CO frequencies of proposed structural models of the active site with that found experimentally. A structure with a hydroxo ligand was proposed for Ni-A, and a water ligand was proposed for Ni-SU,^[56] both models also feature a protonated terminal thiolate. In a later contribution, they revised their assignment and proposed that both states have a hydroxo bridge and an oxygenated thiolate (i.e., sulfenate) group, although a hydroperoxo species for Ni-A was also considered quite possible.^[57] In 2006, the divalent states were investigated, and calculations of the stretching frequency were performed on an inhibited form of the enzyme with an exogenous CO ligand bound to nickel for both the low-spin ($S=0$) and high-spin ($S=1$) configurations; these were found to be similar in terms of energy.^[58] Based on these and other studies, including EPR studies, multiple groups proposed mechanisms for the activation of the enzyme, as well as for the turnover of molecular hydrogen.^[12–17] These mechanisms generally agree with each other, but also exhibit subtle differences, for example, with respect to the protonation state of some redox intermediates. Very recently, it has been convincingly shown that it is essential to take into account the hydrogen bonds of the second coordination sphere to the diatomic ligands in order to reproduce the stretching frequencies; omission leads to deviations of up to 30 cm^{-1} .^[59] A summary of mechanistic studies can be found in reviews by Siegbahn et al.^[60] and Bruschi et al.^[15]

At present, only the Ni-B and Ni-C states are structurally well characterized, in particular by X-ray crystallography and EPR spectroscopy. Moreover, given the complexity of the problem of structurally identifying the redox intermediates of the catalytic mechanism, it becomes particularly apparent (from the variety of proposed structures present in literature) that it is essential to validate the proposed structures with as many available spectroscopic properties as possible. In this contribution, we attempted such a study, with the emphasis on the divalent EPR-silent redox states of the protein, while using the well-characterized structures for Ni-B and Ni-C as references.

Results and Discussion

In order to validate the calculation of the stretching frequencies of diatomic ligands in the hydrogenase models, initial calculations were performed for models of the Ni-B ($X=\text{OH}^-$) and Ni-C ($X=\text{H}^-$) redox states (see Scheme 2). These models include the second coordination sphere and, especially important, the hydrogen bonds to the cyanide ligands. For Ni-C, this model has recently been shown to accurately reproduce all presently known EPR parameters.^[59] The experimentally observed CO and CN frequencies are 1961 , 2074 , and 2085 cm^{-1} , respectively.^[34] The calculated frequencies (1936 , 2055 , and 2080 cm^{-1}) differ by up to 25 cm^{-1} from the experimental data (see Table 2). At present, this is typical for the accuracy to



X	n	S	state
H^-	2	1/2	Ni-C
OH^-	2	1/2	Ni-B ^{a)}
\square	2	0 or 1	Ni-SI
OH^-	3	0 or 1	Ni-SI
H_2O	2	0 or 1	Ni-SI
H^-	3	0 or 1	Ni-R
$\eta^2\text{-H}_2^{\text{b)}$	2	0 or 1	Ni-R

^{a)} no protonation on $\text{S}_\gamma(\text{Cys})$

^{b)} coordination to Ni or Fe

Scheme 2. Active-site models used in this study. X represents the variable bridging position between nickel and iron, n is the total charge, and S is the total spin of the system. The secondary coordination sphere has been omitted for clarity.

which stretching frequencies of CO and CN can be calculated. In particular, Jonas et al. found that the metal–carbonyl stretching frequencies are systematically underestimated in DFT calculations, and proposed a corrective procedure: adding a shift of about 28 cm^{-1} to the calculated values.^[78,79] Such a shift would adjust the calculated CO frequency to 1964 cm^{-1} , thus bringing the number within only a few wavenumbers of the experimental data.

Rather than relying on corrective procedures to eliminate systematic errors, the fact that the Ni-B state has also been well characterized can be exploited. Calculations with the model for Ni-B gave stretching frequencies of 1931 , 2059 , and 2082 cm^{-1} . More importantly, the relative shifts with respect to Ni-C amounted to -5 , $+4$, and $+2\text{ cm}^{-1}$, which is in very good agreement with the experimentally observed frequency differences (-6 , $+7$, and $+5\text{ cm}^{-1}$). Thus, by looking at the change in frequency when using the well-characterized Ni-C state as a reference, systematic errors are eliminated. The good agreement for the shifts of the stretching frequencies for Ni-B with respect to Ni-C is in full agreement with the assignment in the literature,^[41,48] and also indicates that the model structures of the Ni-B and Ni-C states ($X=\text{OH}^-$ and $X=\text{H}^-$, respectively) are sufficiently large. As a final note, we also considered the possibility of protonated terminal cysteines in Ni-C (Table 3). As protonation decreases the backbonding into the CO/CN ligand set, the frequencies of the CN and CO vibrations experience an upward shift of about 20 cm^{-1} relative to the unprotonated form; this is incompatible with the experimental data.

Table 2. Calculated stretching frequencies (cm^{-1}) of the CO and CN vibrations in model structures in which all cysteine residues are modeled as thiolates (unprotonated models). For each model, the total spin S and the identity of the bridging ligand X is specified. The numbers in brackets are the shifts [cm^{-1}] compared to the Ni-C model.

	Ni-B		Ni-C		Ni-SI			
	X=OH ⁻		X=H ⁻		X=OH ⁻		X=H ₂ O	
	$S=1/2$		$S=1/2$		$S=0$	$S=1$	$S=0$	$S=1$
CO	1931 (-5)		1936		1896 (-40)	1898 (-38)	1898 (-38)	1942 (+6)
CN	2059 (+4)		2055		2023 (-32)	2027 (-28)	2026 (-29)	2053 (-2)
CN	2082 (+2)		2080		2054 (-26)	2056 (-24)	2056 (-24)	2082 (+2)

	X=vacant		Ni-R		X=H ₂ O	
	$S=0$	$S=1$	$S=0$	$S=1$	$S=0$	$S=1$
CO	1913 (-23)	1924 (-12)	1896 (-40)	1898 (-38)	1898 (-38)	1942 (+6)
CN	2044 (-11)	2052 (-3)	2023 (-32)	2027 (-28)	2026 (-29)	2053 (-2)
CN	2069 (-11)	2073 (-7)	2054 (-26)	2056 (-24)	2056 (-24)	2082 (+2)

	X=H ⁻		X=η ² -H ₂ (Ni-coordinated)		X=η ² -H ₂ (Fe-coordinated)	
	$S=0$	$S=1$	$S=0$	$S=1$	$S=0$	$S=1$
CO	1899 (-37)	1883 (-53)	1926 (-10)	1929 (-7)	1962 (+26)	1972 (+36)
CN	2014 (-39)	2011 (-44)	2048 (-7)	2051 (-4)	2064 (+9)	2072 (+17)
CN	2050 (-30)	2041 (-39)	2075 (-5)	2075 (-5)	2095 (+15)	2098 (+18)

Table 3. Calculated stretching frequencies [cm^{-1}] of the CO and CN vibrations in model structures in which three cysteine residues are modeled as thiolates and one is a thiol (protonated models). For each model, the identity of the bridging ligand X and the number of the protonated cysteine residue is given.

	Ni-C		Ni-SI			
	X=H ⁻		X=OH ⁻			
	HSγ(Cys81)	HSγ(Cys546)	HSγ(Cys81)	HSγ(Cys81)	HSγ(Cys546)	HSγ(Cys546)
	$S=1/2$	$S=1/2$	$S=0$	$S=1$	$S=0$	$S=1$
CO	1957	1964	1916 (-20)	1915 (-21)	1918 (-18)	1921 (-15)
CN	2077	2078	2042 (-13)	2048 (-7)	2044 (-11)	2045 (-10)
CN	2097	2097	2069 (-11)	2073 (-7)	2068 (-12)	2070 (-10)

	X=vacant		X=H ₂ O		X=vacant	
	HSγ(Cys81)	HSγ(Cys546)	HSγ(Cys81)	HSγ(Cys546)	HSγ(Cys546)	HSγ(Cys546)
	$S=0$	$S=1$	$S=0$	$S=0$	$S=0$	$S=1$
CO	1939 (+3)	1935 (-1)	1927 (-9)	1926 (-10)	1947 (+11)	1951 (+15)
CN	2068 (+13)	2062 (+7)	2050 (-5)	2047 (-8)	2065 (+10)	2070 (+15)
CN	2088 (+8)	2082 (+2)	2077 (-3)	2071 (-9)	2087 (+7)	2088 (+8)

	HSγ(Cys81), X=H ⁻		Ni-R		HSγ(Cys546), X=η ² -H ₂ (Ni)	
	$S=0$	$S=1$	$S=0$	$S=1$	$S=0$	$S=1$
CO	1923 (-13)	1907 (-29)	1923 (-13)	1914 (-22)	1950 (+14)	1949 (+13)
CN	2039 (-16)	2035 (-20)	2039 (-16)	2034 (-21)	2068 (+13)	2066 (+11)
CN	2070 (-10)	2061 (-19)	2066 (-14)	2059 (-21)	2089 (+9)	2085 (+5)

Ni-SI_a and Ni-SI_r

The Ni-SI_a state is oxidized by one electron relative to Ni-C. As such, it is on the same oxidation level as the silent-ready (Ni-SI_r) and silent-unready (Ni-SU) states. The Ni-SI_a state is believed to be the most-oxidized redox state that participates in the catalytic turnover of molecular hydrogen. No crystal structure is available, and, as for the nickel resides in the formal di-

valent (d^8) oxidation state, no data from EPR spectroscopy is available. It is known, however, that protonation equilibrium exists between the Ni-SI_a and Ni-SI_r states, such that the Ni-SI_a state carries one proton more than Ni-SI_r.^[29,30]

Ni-SI_r has been characterized experimentally with a spectacular shift of the CO stretching frequency (by -40 cm^{-1}) and downshifts of the two CN vibrations (-13 and -15 cm^{-1}), compared to Ni-C. The lowered stretching frequencies of all three diatomic ligands are indicative of weakened bonds in all diatomic ligands, as a result of increased π backdonation of electron density from iron to all diatomic ligands. In other words, the experimentally observed downshifts for Ni-SI_r (compared to Ni-C) reflect the increased electron density at the iron (i.e., the charge at the iron is slightly more negative in Ni-SI_r than in Ni-C). The large experimentally observed downshift of the CO frequency of Ni-SI_r was reflected in the models with $X=\text{OH}^-$, $X=\text{H}_2\text{O}$ ($S=0$), and $X=\text{H}^-$. The calculated shifts of the CN frequencies in these models (relative to those in the Ni-C model) are somewhat larger than the experimentally observed shifts (up to 20 cm^{-1}). This discrepancy is particularly large for the model with $X=\text{H}^-$, thus making the latter an unlikely candidate for the Ni-SI_r state.

The Ni-SI_a state displays experimental shifts relative to Ni-C (-8 , 0 , and $+1 \text{ cm}^{-1}$) that are much smaller than those for Ni-SI_r. This trend was reproduced in the models with $X=\text{OH}^-$ and

H_2O , and either of the terminal cysteines (Cys546 or Cys81) protonated. In fact, the experimentally observed frequency differences between Ni-SI_r and Ni-SI_a ($+22$, $+13$, $+16 \text{ cm}^{-1}$) were matched to within 8 cm^{-1} by these models. This observation is completely consistent with previous experiments in which the Ni-SI_a state was deduced to be protonated with respect to Ni-SI_r.^[29,30]

The stretching frequencies (in particular, their shifts from Ni-SI_r to Ni-SI_a) were well reproduced in models for which X is either OH⁻ or H₂O with unprotonated cysteines for Ni-SI_r, and for which X is conserved and one of the terminal cysteines becomes protonated to obtain Ni-SI_a. Based on FTIR frequencies alone, no further discrimination can be made between these two. This unfortunate situation is partly attributable to the fact that, in particular, the poorly reproduced stretching frequencies of the CN ligands are influenced (by up to 30 cm⁻¹) by the hydrogen bonds in the second coordination sphere. Whether inclusion of the second coordination sphere is sufficient for accurate calculation of the CN stretching frequencies (or whether parts of the third coordination sphere have to be taken into account) is presently unclear and beyond the scope of this work.

With the present models indicating protonation of one of the terminal cysteines upon transition from Ni-SI_r to Ni-SI_a, the interesting question arises as to whether protonation of one of these cysteines is energetically favorable if OH⁻ is present. Strikingly, geometry optimization of the model with divalent nickel and X=H₂O in the singlet state (*S*=0) resulted in dissociation of H₂O from iron. In its optimized position, the water molecule only coordinates to nickel, thus rendering the coordination spheres of both metal ions square-pyramidal (Figure 2).

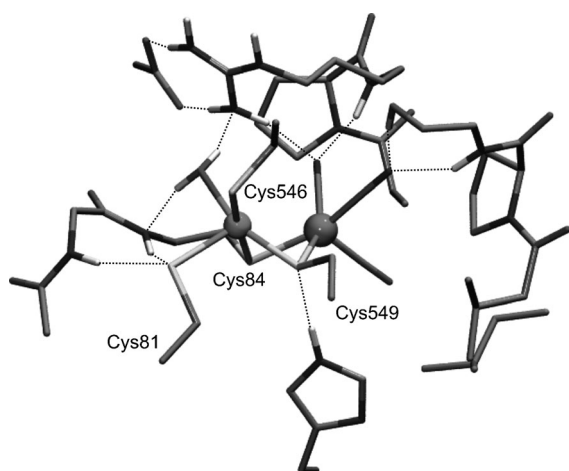


Figure 2. Optimized geometry of the singlet (*S*=0) ground state of the Ni-SI_r cluster model with X=H₂O, Ni^{II}(H₂O)Fe^{II}. Aliphatic hydrogen atoms have been omitted for clarity.

The water ligand resides in the equatorial plane of the square pyramid, together with Cys84, Cys546, and Cys549 (bond distances: Ni–O 2.16 Å, Ni–S 2.21–2.30 Å); Cys81 occupies the apical position (Ni–S 2.36 Å). The Ni–Fe distance amounts to 2.79 Å.

The BP86 calculations indicated that the structures with X=OH⁻ and either of the terminal cysteines protonated are less stable (by 10–15 kcal mol⁻¹) than the structure with the loosely coordinated H₂O. This theoretical analysis indicates that protonation of one of the cysteines is energetically less favorable than protonation of a hydroxo bridging ligand.

A final piece of information again comes from the experimental data. Experiments have indicated that the reduction Ni-B (for which the bridging ligand is OH⁻) is pH dependent, thus suggesting that the reduction involves proton-coupled electron transfer. A picture thus emerges in which Ni-B carries a hydroxo bridging ligand, Ni-SI_r is one-electron reduced and protonated with respect to Ni-B, and Ni-SI_a is protonated with respect to Ni-SI_r. The infrared frequencies are fully compatible with this, and the only set of models compatible with these boundary conditions set by experimentation is the one in which the Ni-SI_r state carries a H₂O molecule, which is weakly coordinated to nickel, and in which Ni-SI_a has essentially the same geometry and includes protonation of one of the terminal cysteines.

Ni-R

The Ni-R states are the most reduced states of the enzyme. Electron density at the bridging ligand X is absent in the crystal structure of Ni-R; this significantly limits the number of possibilities for the bridging ligand. In our models, a hydride bridge or either a nickel- or iron-coordinated H₂ molecule was considered, in combination with protonation of one of the terminal thiolates. Experimentally, multiple fingerprints of stretching frequencies of the Ni-R state have been found; their relative intensities depended on pH. Whether this is a result of a different protonation of the active site, or whether changes in the protonation of the enzyme causes changes in the tertiary structure (and thereby in the structure of the active site) is not resolved. For this reason, we focused on the fingerprint of frequencies assigned to Ni-R that dominates the spectrum at neutral pH. For *D. vulgaris* Miyazaki F, these frequencies occur at 1948, 2061, and 2074 cm⁻¹.^[30] Relative to the Ni-C state, the CO stretching frequency is lower by 5 cm⁻¹ and the CN frequencies are lower by 13 and 11 cm⁻¹.

The model for Ni-R with a hydride bridge and unprotonated thiolates exhibited large downshifts of both the CO (37 cm⁻¹ for *S*=0, 53 cm⁻¹ for *S*=1) and CN stretching frequencies; these are not compatible with experimental data. Three models yielded stretching frequencies that are compatible with the experimentally observed shifts: one where nickel is coordinated by molecular hydrogen (Table 2) and others where nickel is diamagnetic, a hydride bridge is present, and one of the two terminal cysteines is protonated (Table 3). Thus, the calculations of the FTIR frequencies excluded the model with a hydride bridge and unprotonated cysteines. Unfortunately, a final assignment based on the FTIR frequencies alone could not be made.

We thus turned to the total energies. All three structures correspond to minima on the potential energy surface. The BP86 energies indicated that the structure with a hydride bridge and protonated Cys546 is energetically favorable. The structure with H₂ bound side-on to nickel is 8 kcal mol⁻¹ higher, and the structure with a hydride and protonated Cys81 is 11 kcal mol⁻¹ higher. Given that the DFT method has limited chemical accuracy (~10 kcal mol⁻¹, in particular with respect to the amount of Hartree–Fock exchange included in the func-

tion; B3LYP gave a different value), the energies from the DFT calculations indicated at most that the states are close together in energy terms. This observation might actually be quite relevant for the mechanism, as the flatness of the potential energy surface allows large movements of atoms: for example, in this case, the heterolytic splitting of the H–H bond at minimum reorganization energy. It is clear from the combination of experimental and theoretical data concerning the FTIR frequencies of Ni-R that two protons are in the active site, either still as molecular hydrogen bound side-on to nickel, or as a hydride bridge and a protonated cysteine—an important piece of information, very relevant for the catalytic mechanism. In order to further validate the presence of a protonated cysteine, experiments on the Ni-R state by FTIR spectroscopy while monitoring the S–H or S–D vibrations (the latter in combination with isotope exchange experiments) might provide further information.

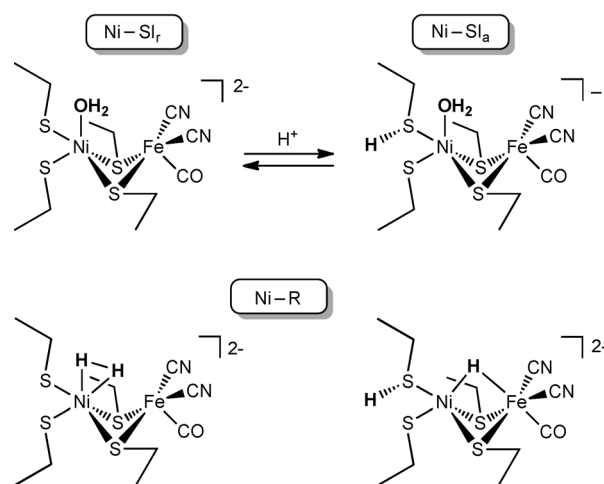
Ni-A and Ni-SU

The silent-unready redox state (Ni-SU) is the one-electron-reduced redox state associated with Ni-A. Although the Ni-A and Ni-B states are characterized by similar FTIR fingerprints, those of Ni-SU and Ni-SI_r states differ. The CO stretching frequency was lower by 3 cm⁻¹ (relative to Ni-C), whereas the CN stretching frequencies increased by about 15 cm⁻¹. Comparison of the experimental FTIR frequencies of Ni-SU with the calculated data in Tables 2 and 3 does not reveal satisfactory agreement. The calculation which comes closest to reproducing experimental data is the one in which the bridge is vacant and Cys81 is protonated. Thus, none of the models, which systematically included only the mildest possible modifications to the geometric structure, gave rise to stretching frequencies compatible with the Ni-SU state. Rather, our observations indicate that a structural rearrangement larger than those represented by the model structures likely occurs upon reduction from Ni-A to Ni-SU. This structural rearrangement would have to be reversed for the activation process of Ni-SU, whereas the Ni-SI_r and Ni-SI_a states are very similar in structure. This is consistent with experimental results, as it is well known that Ni-SI_r is indeed more easily activated than Ni-SU.^[43]

We briefly consider the Ni-A state. Of all paramagnetic redox states, only the Ni-A state is still controversial, with a bridging ligand reported to be initially an S²⁻.^[80] A later proposal featured an OOH⁻ bridge, based on more refined crystal structures,^[22,25] although an even more recent crystal structure for the [NiFe] hydrogenase of *Allochromatium vinosum* again indicates the presence of a mono-oxygen ligand.^[26] As water does not remain coordinated to iron in the divalent nickel state, and EPR experiments of Ni-A have shown that the bridging ligand is associated with at least one proton,^[53] the present data (including the similar fingerprints of Ni-A and Ni-B in the FTIR spectra) seem to favor a hydroxo ligand for Ni-A, just as for Ni-B. Single-crystal ENDOR experiments of the Ni-A state are presently in progress in our laboratory and might shed more light on the exact geometric structure of Ni-A.

Conclusion

In this work, a systematic investigation by quantum chemical methods has been performed for the EPR-silent redox states of [NiFe] hydrogenases, by focusing on computation of the CO and CN stretching frequencies of the inorganic diatomic ligands of iron. The models used geometries that incorporate different bridging ligands (absent, OH⁻, H₂O, H⁻, H₂ bound to either nickel or iron) and protonation of one of the cysteine residues. As such, the model systems have only the mildest possible variations of geometric structure of the [NiFe] center. By comparison of the calculated FTIR frequencies with experiment data of the structurally well-characterized Ni-C and Ni-B states, and by employing a synergistic approach in which a maximum of noncontroversial additional experimental data was included in the analysis, structural pictures for the EPR-silent states emerged (Scheme 3).



Scheme 3. Proposed structures for the Ni-SI and Ni-R states based on calculated CN and CO stretching frequencies.

The Ni-SI_r and Ni-SI_a states feature a water molecule loosely bound to nickel and a formally vacant bridge. The Ni-SI_a state contains one protonated thiolate, whereas the Ni-SI_r state has unprotonated thiolates. The reduced Ni-R state that dominates at neutral pH contains two protons, either bound side-on as H₂ to nickel, or as a hydride bridge and a protonated thiolate. The structures have been found to be isoenergetic within the accuracy of the employed DFT method, thus indicating that upon heterolytic splitting of the H–H bond, the hydride and proton are separated at a minimum cost in terms of reorganization energy. For Ni-SU a clear match between experimentally observed frequencies and those from calculations of the employed models was found, thus indicating that a larger structural arrangement might occur upon reduction from Ni-A to Ni-SU, and that the bridging ligand might dissociate. This rearrangement likely has to be undone before Ni-SU can be activated and might relate to the longer activation time of Ni-SU compared to Ni-SI_r.

When comparing our results with proposed structures for the intermediates and reaction mechanisms postulated by different groups,^[13,14,17] it became clear that all mechanisms agree on the general structures of the intermediates and differ mainly in details concerning the protonation state of the cysteines. Our proposed structures for the intermediates are corroborated by FTIR spectroscopy and represent a cross-section from each proposed mechanism present in the literature. Moreover, the reaction mechanism itself likely consists of more than just the isolatable Ni-SI, Ni-C, and Ni-R states. For a formulation based on experimental and theoretical data of the full reaction mechanism (including its reversible character, which is beyond the scope of this work), it might well be important to include aspects of the transport channels of the protons and molecular hydrogen as well as of the electron transport chain ([FeS] clusters).

Another still-unresolved issue concerns the identities of the Ni-A and Ni-SU states. Investigation of these species by EPR spectroscopy and high-resolution X-ray crystallography is presently in progress in our laboratories.

Experimental Section

The computational active-site model (Figure 1) is a modified version of the large HisH_e cluster model for the Ni-C state of [NiFe] hydrogenase reported by Kampa et al.^[59] The initial geometry was prepared from the crystal structure of *D. vulgaris* Miyazaki F hydrogenase in its reduced form (PDB ID: 1H2R).^[23] The primary coordination sphere involves the active site with the two metal ions (Fe and Ni), two CN⁻ and one CO ligand coordinating the iron, as well as four cysteines. In the starting geometry for Ni-C, the bridging position between the metal ions is occupied by a hydride ligand. The coordination geometry of the Ni center is distorted square-pyramidal, with Cys549 occupying the apical position; the remaining cysteines and the fifth ligand span the equatorial plane. Residues Cys81 and Cys546 bind terminally to the Ni center, while Cys84 and Cys549 adopt bridging positions between the two metal atoms. Apart from Cys84, which forms part of a peptide chain (see below), cysteines were modeled as ethylthiolates. The secondary coordination sphere includes three tripeptide fragments, Gly82–Val83–Cys84, Ala477–Pro478–Arg479, and Val500–Pro501–Ser502, as well as the individual residues His88, Asp123, and Leu482. By incorporation of these nearest amino acids into the model, important secondary interactions (H-bonding, steric) with the core region are maintained (see Figure 1); this has a direct influence on the electronic structure of the active site.^[2] The residues were truncated at the α -carbon atoms (except for Asp123, which was cut at β -C) and saturated with hydrogen atoms. The α -C atoms were constrained to their positions in the X-ray structure during geometry optimization, in order to mimic the structural influence of the enzyme backbone. Asp123 was fixed at its β -C atom; Val83 and Arg479 were left unconstrained. Note also that the isopropyl side-chain of Val83 was truncated, as it imposes no obvious steric strain on the active site. However, by incorporating the peptide fragment in this region of the active site, H-bonding between the backbone and S γ (Cys81) is conserved. In contrast to the HisH_e cluster model (Kampa et al.),^[59] Glu34 and the backbone fragment of Ala548 were included in the present model. Furthermore, a different truncation scheme was used, such that Pro478, Ala477, and Val500 were incorporated into extended peptide chains and no truncations were applied to their respective side chains.

The geometry of the Ni-C model was used as basis for constructing the additional cluster models (Scheme 2). In the Ni-B model, the bridging hydride was replaced by a hydroxo ligand. Both these states were calculated in their doublet ($S=1/2$) ground states (low spin Ni^{II}). In order to probe possible candidates for the Ni-SI and Ni-R states, we studied sets of active-site models with minimum variations, either containing hydroxyl (OH⁻), water (H₂O), hydride (H⁻), or dihydrogen (η^2 -H₂) groups as bridging ligands, or in which the bridging coordination position is unoccupied (\square in Scheme 2). Additionally, we varied the single protonation state of either of the two terminal cysteines (Cys81 or Cys546). For these EPR-silent states we considered both low-spin ($S=0$) and high-spin ($S=1$) states for Ni^{II} in the calculations.

All electronic structure calculations presented in this paper were performed with the ORCA program package.^[61] Geometry optimizations and frequency calculations were carried out at the DFT level; in both cases this used the BP86 GGA functional^[62,63] in conjunction with the RI-J approximation.^[64,65] Final single-point energies were also computed, with the B3LYP hybrid functional^[66–69] combined with the RIJCOSx method.^[70] All calculations employed the def2-TZVPP basis set on both metal atoms and on the atoms in the immediate coordinating sphere, including CN⁻ and CO, S γ of cysteines, and the variable ligand (OH⁻, H₂O, H⁻, H₂). The remaining atoms in the surrounding space were treated with the def2-SV(P) basis set. The segmented all-electron relativistically contracted (SARC) def2 bases were used.^[71] Scalar relativistic effects were incorporated by the all-electron zeroth-order regular approximation (ZORA).^[72–74] Dispersion effects were accounted for by the use of Grimme's empirical van der Waals correction (VDW10).^[75] Dielectric effects of the enzyme environment were approximated by embedding the clusters in a conductor-like screening model (COSMO) with a dielectric constant of $\epsilon=4$.^[76,77] However, solvation was not taken into account for vibrational frequency calculations.

Acknowledgements

The authors thank Dr. Hideaki Ogata for helpful discussions. This work has been performed with financial aid from the Max Planck Gesellschaft (MPG).

Keywords: Computational chemistry · Enzyme models · Metalloenzymes

- [1] P. M. Vignais, B. Billoud, J. Meyer, *FEMS Microbiol. Rev.* **2001**, *25*, 455–501.
- [2] R. Cammack, *Nature* **1999**, *397*, 214–215.
- [3] K. A. Vincent, J. A. Cracknell, A. Parkin, F. A. Armstrong, *Dalton Trans.* **2005**, 3397–3403.
- [4] H. R. Pershad, J. L. C. Duff, H. A. Heering, E. C. Duin, S. P. J. Albracht, F. A. Armstrong, *Biochemistry* **1999**, *38*, 8992–8999.
- [5] A. K. Jones, E. Sillery, S. P. J. Albracht, F. A. Armstrong, *Chem. Commun.* **2002**, 866–867.
- [6] A. K. Jones, S. E. Lamle, H. R. Pershad, K. A. Vincent, S. P. J. Albracht, F. A. Armstrong, *J. Am. Chem. Soc.* **2003**, *125*, 8505–8514.
- [7] C. Léger, A. K. Jones, W. Roseboom, S. P. J. Albracht, F. A. Armstrong, *Biochemistry* **2002**, *41*, 15736–15746.
- [8] C. Léger, A. K. Jones, S. P. J. Albracht, F. A. Armstrong, *J. Phys. Chem. B* **2002**, *106*, 13058–13063.
- [9] S. E. Lamle, S. P. J. Albracht, F. A. Armstrong, *J. Am. Chem. Soc.* **2004**, *126*, 14899–14909.
- [10] K. A. Vincent, A. Parkin, O. Lenz, S. P. J. Albracht, J. C. Fontecilla-Camps, R. Cammack, B. Friedrich, F. A. Armstrong, *J. Am. Chem. Soc.* **2005**, *127*, 18179–18189.

- [11] H. Ogata, W. Lubitz, Y. Higuchi, *Dalton Trans.* **2009**, 7577–7587.
- [12] P. E. M. Siegbahn, M. R. A. Blomberg, M. W. N. Pavlov, R. H. Crabtree, *J. Biol. Inorg. Chem.* **2001**, *6*, 460–466.
- [13] M. Stein, W. Lubitz, *J. Inorg. Biochem.* **2004**, *98*, 862–877.
- [14] L. De Gioia, P. Fantucci, B. Guigliarelli, P. Bertrand, *Inorg. Chem.* **1999**, *38*, 2658–2662.
- [15] M. Bruschi, G. Zampella, P. Fantucci, L. De Gioia, *Coord. Chem. Rev.* **2005**, *249*, 1620–1640.
- [16] P. Amara, A. Volbeda, J. C. Fontecilla-Camps, M. J. Field, *J. Am. Chem. Soc.* **1999**, *121*, 4468–4477.
- [17] M. Pavlov, P. E. M. Siegbahn, M. R. A. Blomberg, R. H. Crabtree, *J. Am. Chem. Soc.* **1998**, *120*, 548–555.
- [18] E. Garcin, X. Vernede, E. C. Hatchikian, A. Volbeda, M. Frey, J. C. Fontecilla-Camps, *Structure* **1999**, *7*, 557–566.
- [19] Y. Montet, P. Amara, A. Volbeda, X. Vernede, E. C. Hatchikian, M. J. Field, M. Frey, J. C. Fontecilla-Camps, *Nat. Struct. Biol.* **1997**, *4*, 523–526.
- [20] A. Volbeda, M. H. Charon, C. Piras, E. C. Hatchikian, M. Frey, J. C. Fontecilla-Camps, *Nature* **1995**, *373*, 580–587.
- [21] A. Volbeda, E. Garcin, C. Piras, A. L. de Lacey, V. M. Fernandez, E. C. Hatchikian, M. Frey, J. C. Fontecilla-Camps, *J. Am. Chem. Soc.* **1996**, *118*, 12989–12996.
- [22] A. Volbeda, L. Martin, C. Cavazza, M. Matho, B. W. Faber, W. Roseboom, S. P. J. Albracht, E. Garcin, M. Rousset, J. C. Fontecilla-Camps, *J. Biol. Inorg. Chem.* **2005**, *10*, 239–249.
- [23] Y. Higuchi, H. Ogata, K. Miki, N. Yasuoka, T. Yagi, *Structure* **1999**, *7*, 549–556.
- [24] H. Ogata, Y. Mizoguchi, N. Mizuno, K. Miki, S. Adachi, N. Yasuoka, T. Yagi, O. Yamauchi, S. Hirota, Y. Higuchi, *J. Am. Chem. Soc.* **2002**, *124*, 11628–11635.
- [25] H. Ogata, S. Hirota, A. Nakahara, H. Komori, N. Shibata, T. Kato, K. Kano, Y. Higuchi, *Structure* **2005**, *13*, 1635–1642.
- [26] H. Ogata, P. Kellers, W. Lubitz, *J. Mol. Biol.* **2010**, *402*, 428–444.
- [27] J. M. C. C. Coremans, C. J. van Garderen, S. P. J. Albracht, *Biochim. Biophys. Acta Protein Struct. Mol. Enzymol.* **1992**, *1119*, 148–156.
- [28] J. M. C. C. Coremans, J. W. van der Zwaan, S. P. J. Albracht, *Biochim. Biophys. Acta Protein Struct. Mol. Enzymol.* **1992**, *1119*, 157–168.
- [29] A. L. de Lacey, E. C. Hatchikian, A. Volbeda, M. Frey, J. C. Fontecilla-Camps, V. M. Fernandez, *J. Am. Chem. Soc.* **1997**, *119*, 7181–7189.
- [30] C. Fichtner, C. Laurich, E. Bothe, W. Lubitz, *Biochemistry* **2006**, *45*, 9706–9716.
- [31] B. Bleijlevens, F. A. van Broekhuizen, A. L. De Lacey, W. Roseboom, V. M. Fernandez, S. P. J. Albracht, *J. Biol. Inorg. Chem.* **2004**, *9*, 743–752.
- [32] B. Bleijlevens, B. W. Faber, S. P. J. Albracht, *J. Biol. Inorg. Chem.* **2001**, *6*, 763–769.
- [33] W. Lubitz, E. Reijerse, M. van Gestel, *Chem. Rev.* **2007**, *107*, 4331–4365.
- [34] M.-E. Pandelia, H. Ogata, W. Lubitz, *ChemPhysChem* **2010**, *11*, 1127–1140.
- [35] S. Kurkin, S. J. George, R. N. F. Thorneley, S. P. J. Albracht, *Biochemistry* **2004**, *43*, 6820–6831.
- [36] S. P. J. Albracht, E. G. Graf, R. K. Thauer, *FEBS Lett.* **1982**, *140*, 311–313.
- [37] H.-J. Krüger, B. H. Huynh, P. O. Ljungdahl, A. V. Xavier, D. V. DerVartanian, I. Moura, H. D. Peck, Jr., M. Teixeira, J. J. G. Moura, J. LeGall, *J. Biol. Chem.* **1982**, *257*, 14620–14623.
- [38] J. J. G. Moura, I. Moura, B. H. Huynh, H.-J. Krüger, M. Teixeira, R. C. DuVarnay, D. V. DerVartanian, A. V. Xavier, H. D. Peck, Jr., J. LeGall, *Biochem. Biophys. Res. Commun.* **1982**, *108*, 1388–1393.
- [39] C. Geßner, O. Trofanchuk, K. Kawagoe, Y. Higuchi, N. Yasuoka, W. Lubitz, *Chem. Phys. Lett.* **1996**, *256*, 518–524.
- [40] O. Trofanchuk, M. Stein, C. Gessner, F. Lenzian, Y. Higuchi, W. Lubitz, *J. Biol. Inorg. Chem.* **2000**, *5*, 36–44.
- [41] M. van Gestel, M. Stein, M. Brecht, O. Schröder, F. Lenzian, R. Bittl, H. Ogata, Y. Higuchi, W. Lubitz, *J. Biol. Inorg. Chem.* **2006**, *11*, 41–51.
- [42] S. J. George, S. Kurkin, R. N. F. Thorneley, S. P. J. Albracht, *Biochemistry* **2004**, *43*, 6808–6819.
- [43] V. M. Fernandez, E. C. Hatchikian, R. Cammack, *Biochim. Biophys. Acta Protein Struct. Mol. Enzymol.* **1985**, *832*, 69–79.
- [44] C. Fan, M. Teixeira, J. Moura, I. Moura, H. B. Hanh, J. Le Gall, H. D. Peck, Jr., B. M. Hoffman, *J. Am. Chem. Soc.* **1991**, *113*, 20–24.
- [45] J. P. Whitehead, R. J. Gurbiel, C. Bagyinka, B. M. Hoffman, M. J. Maroney, *J. Am. Chem. Soc.* **1993**, *115*, 5629–5635.
- [46] M. Carepo, D. L. Tierney, C. D. Brondino, T. C. Yang, A. Pamplona, J. Telsler, I. Moura, J. J. G. Moura, B. M. Hoffman, *J. Am. Chem. Soc.* **2002**, *124*, 281–286.
- [47] A. Goenka-Agrawal, M. van Gestel, W. Gärtner, W. Lubitz, *J. Phys. Chem. B* **2006**, *110*, 8142–8150.
- [48] M. Brecht, M. van Gestel, T. Bührke, B. Friedrich, W. Lubitz, *J. Am. Chem. Soc.* **2003**, *125*, 13075–13083.
- [49] M. Flores, A. Goenka-Agrawal, M. van Gestel, W. Gärtner, W. Lubitz, *J. Am. Chem. Soc.* **2008**, *130*, 2402–2403.
- [50] S. Foerster, M. Stein, M. Brecht, H. Ogata, Y. Higuchi, W. Lubitz, *J. Am. Chem. Soc.* **2003**, *125*, 83–93.
- [51] S. Foerster, M. van Gestel, M. Brecht, W. Lubitz, *J. Biol. Inorg. Chem.* **2005**, *10*, 51–62.
- [52] M. E. Pandelia, P. Infossi, M. Stein, M. T. Giudici-Ortoni, W. Lubitz, *Chem. Commun.* **2012**, *48*, 823–825.
- [53] M. van Gestel, C. Fichtner, F. Neese, W. Lubitz, *Biochem. Soc. Trans.* **2005**, *33*, 7–11.
- [54] Y. Nicolet, C. Piras, P. Legrand, C. E. Hatchikian, J. C. Fontecilla-Camps, *Structure* **1999**, *7*, 13–23.
- [55] S. Q. Niu, L. M. Thomson, M. B. Hall, *J. Am. Chem. Soc.* **1999**, *121*, 4000–4007.
- [56] S. Li, M. B. Hall, *Inorg. Chem.* **2001**, *40*, 18–24.
- [57] A. Pardo, A. L. De Lacey, V. M. Fernández, Y. Fan, M. B. Hall, *J. Biol. Inorg. Chem.* **2007**, *12*, 751–760.
- [58] A. Pardo, A. L. De Lacey, V. M. Fernandez, H.-J. Fan, Y. Fan, M. B. Hall, *J. Biol. Inorg. Chem.* **2006**, *11*, 286–306.
- [59] M. Kampa, W. Lubitz, M. van Gestel, F. Neese, *J. Biol. Inorg. Chem.* **2012**, *17*, 1269–1281.
- [60] P. E. M. Siegbahn, J. W. Tye, M. B. Hall, *Chem. Rev.* **2007**, *107*, 4414–4435.
- [61] F. Neese, ORCA, An ab initio, DFT and semiempirical SCF-MO package 2.9.0 R3002, MPI for Chemical Energy Conversion, **2013**.
- [62] A. D. Becke, *Phys. Rev. A* **1988**, *38*, 3098–3100.
- [63] J. P. Perdew, *Phys. Rev. B* **1986**, *33*, 8822–8824.
- [64] E. J. Baerends, D. E. Ellis, P. Ros, *Chem. Phys.* **1973**, *2*, 41–51.
- [65] B. I. Dunlap, J. W. D. Connolly, J. R. Sabin, *J. Chem. Phys.* **1979**, *71*, 3396–3402.
- [66] A. D. Becke, *J. Chem. Phys.* **1993**, *98*, 5648–5652.
- [67] C. Lee, W. Yang, R. G. Parr, *Phys. Rev. B* **1988**, *37*, 785–789.
- [68] S. H. Vosko, L. Wilk, M. Nusair, *Can. J. Phys.* **1980**, *58*, 1200–1211.
- [69] P. J. Stephens, F. J. Devlin, C. F. Chabalowski, M. J. Frisch, *J. Phys. Chem.* **1994**, *98*, 11623–11627.
- [70] F. Neese, F. Wennmohs, A. Hansen, U. Becker, *Chem. Phys.* **2009**, *356*, 98–109.
- [71] D. A. Pantazis, X.-Y. Chen, C. R. Landis, F. Neese, *J. Chem. Theory Comput.* **2008**, *4*, 908–919.
- [72] E. van Lenthe, J. G. Snijders, E. J. Baerends, *J. Chem. Phys.* **1996**, *105*, 6505–6516.
- [73] E. van Lenthe, A. van der Avoird, P. E. S. Wormer, *J. Chem. Phys.* **1998**, *108*, 4783–4796.
- [74] C. van Wüllen, *J. Chem. Phys.* **1998**, *109*, 392–399.
- [75] S. Grimme, J. Antony, S. Ehrlich, H. Krieg, *J. Chem. Phys.* **2010**, *132*, 154104.
- [76] A. Klamt, G. Schüürmann, *J. Chem. Soc. Perkin Trans. 2* **1993**, 799–805.
- [77] S. Sinnecker, A. Rajendran, A. Klamt, M. Diedenhofen, F. Neese, *J. Phys. Chem. A* **2006**, *110*, 2235–2245.
- [78] V. Jonas, W. Thiel, *J. Chem. Phys.* **1995**, *102*, 8474–8484.
- [79] V. Jonas, W. Thiel, *Organometallics* **1998**, *17*, 353–360.
- [80] Y. Higuchi, T. Yagi, N. Yasuoka, *Structure* **1997**, *5*, 1671–1680.

Received: February 26, 2013

Published online on May 22, 2013